



Cite this: *Chem. Commun.*, 2025, 61, 14129

Received 21st April 2025,
Accepted 7th August 2025

DOI: 10.1039/d5cc02180d

rsc.li/chemcomm

On metal–organic framework isomers, and the SF₆ sorption and fluorescence of an In and a Zr MOF with a tritopic linker†

Hao Li,^a Francoise M. Amombo Noa, ^{id}*^{ab} Michelle Åhlén, ^{id}^c Zhejian Cao, ^{id}^d Joakim Andréasson, ^{id}^a Ocean Cheung ^{id}^c and Lars Öhrström ^{id}*^a

The concept of framework isomers by network topology analysis is illustrated by a new rod-MOF isomer of In³⁺ and the tritopic linker 4,4',4''-(benzene-1,3,5-triyl-tris(oxy))tribenzoic acid (H₃bttb), CTH-41, with a unique 3- and 4-connected net different from 437-MOF. CTH-41 shows affinity for SF₆ with a Langmuir area of 1587 m² g⁻¹ while the new Zr⁴⁺ dot-MOF with the same linker [Zr₆(bttb)₄(O)₄(OH)₄] CTH-42, forms the 3-, 12-connected IIj-net based on a different conformation of the flexible bttb linker.

The discovery and determination of molecular isomers were essential for the development of organic chemistry 200 years ago, and coordination chemistry some 80 years later. Polymorphism can be viewed as the solid state analogue, and was also discovered in the 1820's.¹ Polymorphs appear when materials with identical composition pack differently in their crystals, yielding different space groups and unit cells.

This also occurs for metal–organic frameworks (MOFs), when identical organic and inorganic secondary building units, SBUs, form topologically distinct networks.^{2,3} The analysis of framework isomerism is as essential for reticular chemistry as it once was for molecular chemistry, and still poorly understood.

We use [In₃(bttb)₂(OH)₃] CTH-41, and 437-MOF to illustrate the importance of MOF framework isomerism, the geometry of SBUs and topology, see Fig. 1. [Zr₆(bttb)₄(O)₄(OH)₄] CTH-42 is not a framework isomer to the previous but will be discussed from another angle.

Zhou and co-authors² define framework isomers as MOFs with different network structures. Framework isomers can also

be structures with similar but distinguishable conformational frameworks arising from different anions and solvents.⁴ The factors that create framework isomerism are typically temperature, solvent or templating molecules, concentrations and pH.⁵ To optimize the synthesis of phase pure materials is a non-trivial task requiring extensive condition screening.^{6–8}

Three groups of framework isomers have been identified.² The first and second are interpenetration isomers and conformational framework isomers. The last one, orientation framework isomers, is rare. These isomers consist of SBUs which, taken as independent entities, are indistinguishable based on atomic makeup, connectivity, symmetry or other factors. They are generated by different orientations of the SBUs within the frameworks,² and can normally be distinguished by their all-nodes network topologies.⁹

Good examples are the PCN-16 and PCN-16' MOFs discussed in ref. 2 where the “single node” deconstruction reported results in the same nbo-net for both MOFs.² However, following the “all nodes” approach⁹ we find that these two MOFs indeed can be described in more detail as the 3- and 4-connected fog and fof nets respectively, see SI.

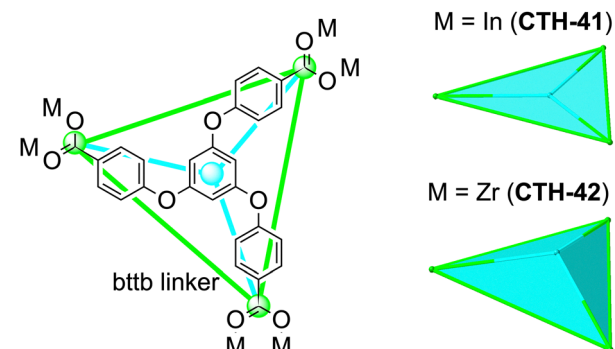


Fig. 1 The linker H₃bttb forming two MOF derivatives, [In₃(bttb)₂(OH)₃] CTH-41, and [Zr₆(bttb)₄(O)₄(OH)₄] CTH-42. The colored points and lines illustrate two limiting symmetric configurations of this flexible linker, the planar triangle as in CTH-41, (all in one plane) and the triangular pyramid (blue point above the plane) as in CTH-42.

^a Chemistry and Biochemistry, Dept. of Chemistry and Chemical Engineering, Chalmers University of Technology, SE-41296 Gothenburg, Sweden.

E-mail: mystere@chalmers.se, ohrstrom@chalmers.se

^b School of Health Sciences, Catholic University of Central Africa, P.O. Box 1110, Yaoundé, Cameroon

^c Department of Materials Science and Engineering, Ångström Laboratory, Uppsala University, SE-751 03 Uppsala, Sweden

^d Department of Life Sciences, Chalmers University of Technology, SE-41296 Gothenburg, Sweden

† Dedicated to the memory of Professor Vratislav Langer 1949–2024.



In this work, we employ the tritopic linker $H_3\text{bttb}$, which often adopts a triangular geometry in the solid state (Fig. 1), as we considered this an excellent candidate for the preparation of MOFs with framework isomers. The bttb linker has flexibility around its ether groups and can adopt several conformations, the two most symmetric being a planar triangle and a triangular pyramid, (Fig. 1), thus in theory producing various topologies.

The other reason for choosing $H_3\text{bttb}$ is that, based on analysis of the Cambridge Structural Database (CSD),¹⁰ most MOFs synthesized with $H_3\text{bttb}$ linker form 1D channels in their frameworks.^{11–13} We find 1D channels preferable as the unidirectional nature of transport reduces cross-diffusion, which can improve separation performance, though it may make membrane fabrication more challenging.^{14,15}

Since bttb^{3–} is a O-terminated hard base ligand according to Hard and Soft Acid and Base (HSAB) theory, we chose to explore MOFs based on its strong interaction with hard Lewis acids, such as high valent Zr^{4+} and In^{3+} metal ions, for the purpose of building stable frameworks built from strong bonds.

Solvothermal synthesis in dimethylacetamide (dma) at 120 °C with $In(NO_3)_3$ gave the rod-MOF $[In_3(\text{bttb})_2(\text{OH})_3]$, **CTH-41** but with $ZrCl_4$ in dimethylformamide (dmf) and acetic acid at 120 °C $[Zr_6(\text{bttb})_4(\text{O})_4(\text{OH})_4]$ **CTH-42** was formed. Both preparations gave crystals suitable for single crystal X-ray diffraction.‡

CTH-41 crystallises in a space group $P\bar{6}2c$ and has not only an identical formula to **437-MOF**¹⁶ synthesised in dmf at 120 °C, but also the SBUs are identical, see Fig. 2.

Packing diagrams (Fig. S3), however, reveal these as two different structures, also reflected in their sorption properties where the derived pore size of **437-MOF** is close to 30 Å whereas in **CTH-41** it is nearer to 12 Å. We speculate that differences in hydrogen bonding, and in In^{3+} solvation, in dmf and dma might be one factor, see SI, Section S12.

Network analysis was used to distinguish between these framework isomers. We note that the network topology of **437-MOF** has previously been described in different ways.^{16,17} We apply here the most reductive method, the straight rod approach (STR) by adding mid-points between the metal ions and connecting the carbon atom of the COO bridge to the midpoint of the rod, (see SI, Section S3).^{18,19}

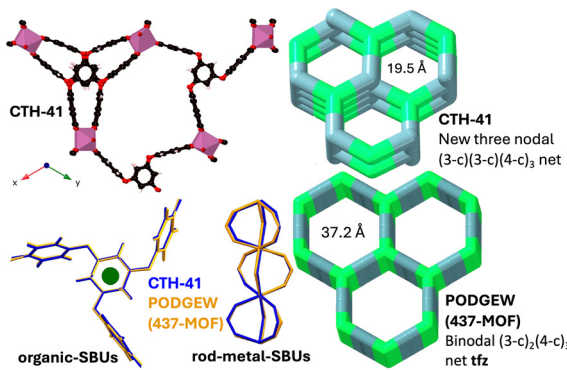


Fig. 2 Left: Crystal structure of $[In_3(\text{bttb})_2(\text{OH})_3]$ **CTH-41**, and superposition of the organic SBUs and metal-SBUs of $[In_3(\text{bttb})_2(\text{OH})_3]$ **CTH-41**, and $[In_3(\text{bttb})_2(\text{OH})_3]$ **437-MOF**. Right: The nets in $[In_3(\text{bttb})_2(\text{OH})_3]$ **CTH-41**, and $[In_3(\text{bttb})_2(\text{OH})_3]$ **437-MOF** using the STR approach. The largest rings in the **CTH-41** net is 8 whereas in **tfz** it is 10 nodes.

This approach now clearly distinguishes the two isomers: **437-MOF** forms the binodal $(3\text{-c})_2(4\text{-c})_3$ **tfz**-net (3- and 4-connected) based on triangles and squares whereas **CTH-41** forms a new trinodal $(3\text{-c})(3\text{-c})(4\text{-c})_3$ net with vertex symbol $(6^3)(8^3)(6^2\cdot8^4)_3$, based on triangles and a see-saw, see Fig. 2. It is obvious that the **tfz**-net allows for larger channels, also indicated by the vertex symbols (SI, Section S3), with the largest rings in the **CTH-41** net being 8-membered, but 10-membered in **tfz**.

The two MOFs **CTH-41** and **437-MOF** are orientational framework isomers,¹⁶ as the structures of the SBUs are near identical (Fig. 2) but they differ in their relative orientations. Specifically, for one linker in **CTH-41** the relative SBU orientation is changed by 180° (Fig. S5) compared to **437-MOF**.

Turning to $[Zr_6(\text{bttb})_4(\text{O})_4(\text{OH})_4]$ **CTH-42**, a classical dot-MOF,²⁰ the question is now what frameworks can be formed from the flexible tritopic bttb linker and the ubiquitous 12-connected $\{Zr_6(\text{CO}_2)_{12}(\text{O})_4(\text{OH})_4\}$ metal-SBU.²¹ The Zr_6 SBU normally forms of a cuboctahedron, a polyhedron with eight triangular and six square faces, that we now shall combine with the triangular SBU of the bttb.

In their survey of reticular chemistry motifs based on the geometry of the SBUs, Kalmutzki *et al.* show the rarity of combining 12-c nodes with triangular SBUs, citing the only examples as the **sky**-net for the cuboctahedron, none for the icosahedron, the **aea**-net for the hexagonal antiprism, and **ttt** for the truncated tetrahedron.²²

A survey of the networks of more than 900 known MOFs based on the Zr_6 coordination entity reveals a striking lack of tritopic linkers, around 3% (see SI, Section S4). In a discussion of 4,12-c Zr-MOFs with 1,3,5,7-tetra(carboxyphenyl) benzene, Nateghi *et al.* noted that they could not obtain a MOF with a corresponding tritopic linker.²³ The well-known MOF-808 on the other hand adopts a 3,6-c **spn** topology by incorporating six formate terminating ligands into the $\{Zr_6(\text{CO}_2)_{12}(\text{O})_4(\text{OH})_4\}$ core.

CTH-42 crystallises in a tetragonal space group $I4/m$ and the Zr_6 cluster indeed forms a cuboctahedron SBU just as in UiO-66.

The structure is shown in Fig. 3 together with the unusual **Ilj**-net that describes the structure. **CTH-42** is a dot-MOF but still has pronounced 1D channels along the z-axis due to the conformation of the bttb linker, distinctively different from what is found in **CTH-41** as illustrated in Fig. S6.

In contrast to the few 3,12-c Zr-MOFs in the CSD, the 4,12-c Zr-MOFs (>20%) are more common which we attribute to the match

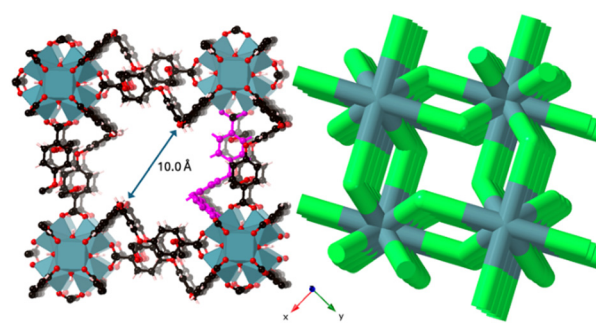


Fig. 3 $[Zr_6(\text{bttb})_4(\text{O})_4(\text{OH})_4]$ **CTH-42** with one bttb linker in pink, and the 3,12-c **Ilj** net describing the structure. The narrowest diameter of the channels in z-direction is given.



between the perfect cuboctahedron of the $\{Zr_6(CO_2)_{12}(O)_4(OH)_4\}$ SBU and a square planar SBU in the **ftw**-net. In contrast there seems to be no known network that combines a perfect cuboctahedron with a perfect triangle.

The eight 3,12-c Zr-MOFs we have identified in the CSD have either the same **llj**-net as **CTH-42**, for example **I-Rh**,²⁴ and **ZrBTE**,²⁵ or the **sky**-net as in **MOF-1004**.²⁶

There is a good agreement of **CTH-41** and **CTH-42** calculated powder X-ray diffraction (PXRD) patterns with their respective as-synthesised bulk materials, illustrated in Fig. S9 and S10. PXRD reveals that **CTH-41** is stable in CH_2Cl_2 , methanol, dmf, and *dma*, but shows peak broadening in water. **CTH-42** loses crystallinity in water, methanol, and CH_2Cl_2 , only retaining framework integrity in dmf, Fig. S10. While **CTH-41** is stable for two years in room temperature **CTH-42** transforms to other phases, thus suggesting an inherent instability of the framework in **CTH-42**.

Elemental analysis and thermogravimetry are consistent with solvent filled channels (SI, Sections S5 and S6) but also some linker deficiency in **CTH-42**, as sometimes observed with the Zr_6 SBU, see SI.²⁷ **CTH-41** and **CTH-42** show disintegration at temperatures above 400 °C and 500 °C respectively.

After synthesis, the MOFs were washed with dmf before solvent exchange at room temperature, first with anhydrous dmf 3 times and then anhydrous methanol 3 times and kept in methanol prior to supercritical CO_2 activation, see SI, Section S1.

The specific Brunauer–Emmett–Teller (BET) and Langmuir areas of **CTH-41** estimated using the N_2 adsorption isotherm were found to be 1378 and 1587 $m^2 g^{-1}$, respectively (Fig. S13(a) and Table S6), in good agreement with the value obtained from the single crystal data using the Mercury²⁸ pore analyser, 1701 $m^2 g^{-1}$. However, for **CTH-42** the BET and Langmuir areas were estimated using CO_2 , as N_2 adsorption kinetics on this framework was very slow, especially at low relative pressure. This gave areas of 305 $m^2 g^{-1}$ and 383 $m^2 g^{-1}$ respectively (Fig. S14(a) and Table S7), considerably lower than predicted by the pore analysis with Mercury, 2652 $m^2 g^{-1}$. Stability issues, as noted above, may be behind this discrepancy, as also the regeneration plot indicates gradual breakdown of **CTH-42** between cycles (Fig. S17).

The pore size distributions were estimated using N_2 (**CTH-41**) and CO_2 (**CTH-42**) isotherms by the slit pore model and density functional theory, as seen in Fig. S13(b) and Fig. S14(b). **CTH-41** showed one type of pore with estimated diameter of approximately 11.8 Å in good agreement with crystallographic data using Mercury, indicating 10.1–10.5 Å. Two distinct types of pores were detected for **CTH-42** with estimated diameters of ~3.6 and ~5.3 Å, in reasonable agreement with the crystal structure showing larger channels of diameter 7.2 Å and a narrower more winding connection of cavities with diameters 4–5 Å. This agreement between experimentally derived pore size and the crystal structure further supports that partial structure collapse is behind the small surface area for **CTH-42**.

The N_2 , CH_4 , SF_6 and CO_2 adsorption isotherms of **CTH-41** and **CTH-42** at 20 °C are shown in Fig. 4, and we want to highlight the greenhouse gas SF_6 . The SF_6 adsorption isotherm of **CTH-41** shows a gradual increase at low pressures, indicating that the pore with approximate diameter of 11.8 Å, which is noticeably larger than the kinetic diameter of SF_6 (5.5 Å), is most likely too large

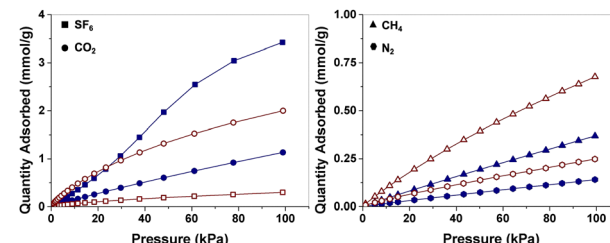


Fig. 4 N_2 , CH_4 , SF_6 and CO_2 adsorption isotherms of **CTH-41** (blue, closed symbols) and **CTH-42** (brown, open symbols) recorded at 20 °C.

for the enhanced SF_6 interaction of other MOFs discussed in our previous studies.^{29,30} The total uptake, however, is reasonably good with more than 3.3 $mmol\ g^{-1}$ at 1 bar and the isosteric heat of sorption is 27.3 to 21.4 $kJ\ mol^{-1}$ (0.05–2.70 $mmol\ g^{-1}$ SF_6 , Fig. S15). It is worth noting that the SF_6 isotherm of **CTH-41** shows an S shape, and that the heat of SF_6 adsorption increases with the SF_6 uptake. This may suggest that with the internal surface of **CTH-41** coated with initially adsorbed SF_6 , the subsequent adsorbent-adsorbate interaction can be enhanced due to partial positive and negative charge separation at the newly formed internal surface from the large electronegativity difference between S and F.

For **CTH-42**, CO_2 uptake was the highest of the tested gases, indicating that **CTH-42** has some selectivity towards CO_2 over the other gases. The uptake at 1 bar (20 °C) reached a moderate 2.0 $mmol\ g^{-1}$ with an isosteric heat of CO_2 sorption of around 21.6–24.2 $kJ\ mol^{-1}$ at up to 1.65 $mmol\ g^{-1}$ loading (Fig. S16).

We also performed cyclic adsorption/desorption experiments on **CTH-41** and **CTH-42** using SF_6 and CO_2 , respectively. **CTH-41** shows complete regenerability over five SF_6 sorption cycles, but the less stable **CTH-42** experienced a decrease of CO_2 uptake of 3–4% per cycle (Fig. S17).

Due to the inherent fluorescence (Fig. S19), **CTH-41** and **CTH-42** were investigated as potential fluorescent sensors for organophosphorus pesticides. While established analysis protocols exist for these compounds, there is a need for off-grid solutions for rapid field tests for first responders, especially as these compounds also mimic, and are related to, chemical weapons such as sarin.^{31,32}

Here, paraoxon methyl (analogue to parathion-methyl) and a non-phosphate pesticide permethrin (Fig. 5) were investigated as they are difficult to monitor by visual inspection, indicated by the UV-Vis spectra of their dmf solutions (Fig. S21). The fluorescence of both MOFs can be quenched by the analyte species, which may have been facilitated by the 1D channels of the MOFs in terms of analyte diffusion and subsequent MOF-analyte interaction. As energy transfer reactions are excluded as the mechanism of quenching (little to zero spectral overlap) the most likely quenching mechanism is photoinduced electron transfer (PET). As **CTH-41** is more stable in solvents than **CTH-42**, only this MOF was further investigated for fluorescence detection properties with the analytes paraoxon methyl and permethrin.

Quantitative data were obtained by dispersing **CTH-41** in dmf and titrating with paraoxon methyl or permethrin, recording the fluorescence intensities (Fig. 5). Stern–Volmer analysis allowed us to determine the limit of detection (LOD) and limit of quantification (LOQ), which are 6.37 μM and 8.44 μM for



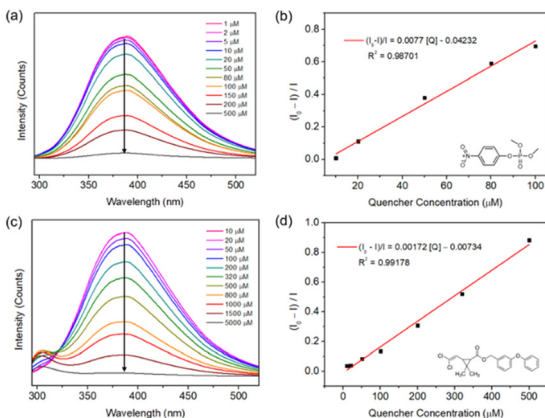


Fig. 5 (a) and (c) Fluorescence emission spectra of **CTH-41** dispersed in dmf titrated with paraoxon methyl or permethrin; (b) and (d) Stern–Volmer fitting of the fluorescence intensities. Excitation for emission readout at 280 nm. For data on **CTH-42** see SI.

paraoxon methyl, and 8.16 μM respectively 17.46 μM for permethrin (SI, Section S11).

This is similar to what was reported for a Cd-bttb MOF with parathion-methyl: LOD of 12 μM and LOQ of 39 μM,¹² demonstrating the capability of **CTH-41** to detect organophosphates and insecticides at a trace level.

In conclusion we have shown the importance of orientation framework isomers by example of $[\text{In}_3(\text{bttb})_2(\text{OH})_3]$ **CTH-41**, and **437-MOF** and how they can be differentiated by network topology analysis. We also noted the high SF_6 capacity of **CTH-41** and the unusual network topology of **CTH-42**, $[\text{Zr}_6(\text{bttb})_4(\text{O})_4(\text{OH})_4]$, and showed the possible quantification of the pesticides paraoxon methyl, and permethrin. Finally, we have explained the puzzling absence of 3,12-c Zr-MOFs by the network topology mismatch between a perfect cuboctahedron and a perfect triangle SBU. We also note further studies are warranted for **CTH-42**. These results show the continued relevance of network topology analysis in reticular chemistry and the possibilities framework isomerism offers for new MOF materials.

Conflicts of interest

There are no conflicts to declare.

Data availability

The data supporting this article have been included as part of the SI, as cif files, and an adsorption information (.aif) format file.

Supplementary information available: Synthesis and characterisation details. See DOI: <https://doi.org/10.1039/d5cc02180d>

CCDC 2444498 and 2444504 contain the supplementary crystallographic data for this paper.^{34,35}

Notes and references

‡ The reported MOFs were characterised by single crystal diffraction PXRD, TGA, SEM, and elemental analysis. Topologies were analysed with SYSTRE.³³ Gas sorption analyses were run on a Micromeritics ASAP2020.

- J. Bernstein, *Polymorphism in Molecular Crystals*, Oxford University Press, New York, USA, 2002.
- T. A. Makal, A. A. Yakovenko and H.-C. Zhou, *J. Phys. Chem. Lett.*, 2011, **2**, 1682–1689.
- L. Öhrström and F. M. Amombo Noa, *Metal-Organic Frameworks*, American Chemical Society, 2020.
- X.-Q. Lü, Y.-Q. Qiao, J.-R. He, M. Pan, B.-S. Kang and C.-Y. Su, *Cryst. Growth Des.*, 2006, **6**, 1910–1914.
- N. Stock and S. Biswas, *Chem. Rev.*, 2012, **112**, 933–969.
- B. Moulton and M. J. Zaworotko, *Chem. Rev.*, 2001, **101**, 1629–1658.
- J.-P. Zhang, X.-C. Huang and X.-M. Chen, *Chem. Soc. Rev.*, 2009, **38**, 2385–2396.
- A. Karmakar, A. Paul and A. J. L. Pombeiro, *CrystEngComm*, 2017, **19**, 4666–4695.
- C. Bonneau, M. O’Keeffe, D. M. Proserpio, V. A. Blatov, S. R. Batten, S. A. Bourne, M. S. Lah, J.-G. Eon, S. T. Hyde, S. B. Wiggins and L. Öhrström, *Cryst. Growth Des.*, 2018, **18**, 3411–3418.
- C. R. Groom, I. J. Bruno, M. P. Lightfoot and S. C. Ward, *Acta Crystallogr., Sect. B*, 2016, **72**, 171–179.
- W. J. Phang, W. R. Lee, K. Yoo, B. Kim and C. S. Hong, *Dalton Trans.*, 2013, **42**, 7850–7853.
- J. Zhang, W. Zhou, L. Zhai, X. Niu and T. Hu, *CrystEngComm*, 2020, **22**, 1050–1056.
- H.-J. Peng, G.-X. Hao, Z.-H. Chu, Y.-W. Lin, X.-M. Lin and Y.-P. Cai, *RSC Adv.*, 2017, **7**, 34104–34109.
- Y. Liu, B. Zhang, D. Liu, P. Sheng and Z. Lai, *J. Membr. Sci.*, 2017, **528**, 46–54.
- Y. Liu, J. Liu and J. Hu, *BMC Chem. Eng.*, 2019, **1**, 3.
- M. Du, M. Chen, X.-G. Yang, J. Wen, X. Wang, S.-M. Fang and C.-S. Liu, *J. Mater. Chem. A*, 2014, **2**, 9828–9834.
- A. Schoedel, M. Li, D. Li, M. O’Keeffe and O. M. Yaghi, *Chem. Rev.*, 2016, **116**, 12466–12535.
- L. S. Xie, E. V. Alexandrov, G. Skorupskii, D. M. Proserpio and M. Dincă, *Chem. Sci.*, 2019, **10**, 8558–8565.
- P. Tshuma, B. C. E. Makhubela, L. Öhrström, S. A. Bourne, N. Chatterjee, I. N. Beas, J. Darkwa and G. Mehlana, *RSC Adv.*, 2020, **10**, 3593–3605.
- F. M. Amombo Noa, M. Abrahamsson, E. Ahlberg, O. Cheung, C. R. Göb, C. J. McKenzie and L. Öhrström, *Chem.*, 2021, **7**, 2491–2512.
- S. Yuan, L. Feng, K. Wang, J. Pang, M. Bosch, C. Lollar, Y. Sun, J. Qin, X. Yang, P. Zhang, Q. Wang, L. Zou, Y. Zhang, L. Zhang, Y. Fang, J. Li and H.-C. Zhou, *Adv. Mater.*, 2018, **30**, 1704303.
- M. J. Kalmutzki, N. Hanikel and O. M. Yaghi, *Sci. Adv.*, 2018, **4**.
- B. Nataf, K. V. Domasevitch, R. Balánek, C. Janiak and I. Boldog, *Inorg. Chem.*, 2019, **58**, 12786–12797.
- T. Sawano, Z. Lin, D. Boures, B. An, C. Wang and W. Lin, *J. Am. Chem. Soc.*, 2016, **138**, 9783–9786.
- S. Won, S. Jeong, D. Kim, J. Seong, J. Lim, D. Moon, S. B. Baek and M. S. Lah, *Chem. Mater.*, 2022, **34**, 273–278.
- S. Lee, H.-B. Bürgi, S. A. Alshimiri and O. M. Yaghi, *J. Am. Chem. Soc.*, 2018, **140**, 8958–8964.
- C. Koschnick, R. Stäglich, T. Scholz, M. W. Terban, A. von Mankowski, G. Savasci, F. Binder, A. Schökel, M. Etter, J. Nuss, R. Siegel, L. S. Germann, C. Ochsenfeld, R. E. Dinnebier, J. Senker and B. V. Lotsch, *Nat. Commun.*, 2021, **12**, 3099.
- C. F. Macrae, I. J. Bruno, J. A. Chisholm, P. R. Edgington, P. McCabe, E. Pidcock, L. Rodriguez-Monge, R. Taylor, J. van de Streek and P. A. Wood, *J. Appl. Crystallogr.*, 2008, **41**, 466–470.
- M. Åhlén, F. M. Amombo Noa, L. Öhrström, D. Hedbom, M. Strömmé and O. Cheung, *Microporous Mesoporous Mater.*, 2022, **343**, 112161.
- F. M. Amombo Noa, O. Cheung, M. Åhlén, E. Ahlberg, P. Nehla, G. Salazar-Alvarez, S. Ersahrad, B. Sanyal and L. Öhrström, *Chem. Commun.*, 2023, **59**, 2106–2109.
- R. Burks and A. Winokur, in *Encyclopedia of Forensic Sciences*, ed. M. M. Houck, Elsevier, Oxford, 2023, pp. 263–277.
- M. J. Kangas, R. Lukowicz, J. Atwater, A. Pliego, Y. Al-Shidfat, S. Havenridge, R. Burks, B. Garver, M. Mayer and A. E. Holmes, *Anal. Chem.*, 2018, **90**, 9990–9996.
- O. Delgado-Friedrichs and M. O’Keeffe, *Acta Crystallogr., Sect. A*, 2003, **59**, 351–360.
- H. Li, F. M. Amombo Noa, M. Åhlén, Z. Cao, J. Andréasson, O. Cheung and L. Öhrström, CCDC 2444498: Experimental Crystal Structure Determination, 2025, DOI: [10.5517/ccdc.csd.cc2n1ps6](https://doi.org/10.5517/ccdc.csd.cc2n1ps6).
- H. Li, F. M. Amombo Noa, M. Åhlén, Z. Cao, J. Andréasson, O. Cheung and L. Öhrström, CCDC 2444504: Experimental Crystal Structure Determination, 2025, DOI: [10.5517/ccdc.csd.cc2n1pzd](https://doi.org/10.5517/ccdc.csd.cc2n1pzd).

